Phytochemicals of mustard leaves tuned the nickel-cobalt bimetallic oxide ($NiCo_2O_4$) properties via particle size reduction towards the development of sensitive and selective enzyme free glucose sensor

Abdul Ghaffar Solangi[1], Tajness Pirzada[1], Aqeel Ahmed Shah[5], Abdul Sattar Chang[2], Zulifqar Ali Solangi[4], Muhammad Yameen Solangi[3], Umair Aftab[3], Matteo Tonezzer[7], Aneela Tahira[2], Shymaa S. Medany[8], Ayman Nafady[6], Zafar Hussain Ibupoto[2]

[1]Institute of Chemistry, Shah Abdul Latif University, Khairpur Mirs 66111, Pakistan

[2]Institute of Chemistry, University of Sindh, Jamshoro 76080, Pakistan

[3]Department of Metallurgy and Materials Engineering, Mehran University of Engineering and Technology, 76080 Jamshoro, Sindh Pakistan

[4]Department of Chemical Engineering, Mehran University of Engineering and Technology, Jamshoro 76020, Pakistan

[5]Department of Metallurgical Engineering, NED University of Engineering and Technology, Karachi, Sindh Pakistan

[6]Department of Chemistry, College of Science, King Saud University, Riyadh 11451, Saudi Arabia

[7] MEM-CNR, Sede di Trento-FBK, Via alla Cascata 56/C, 38123 Trento, Italy

[8]Depatment of Chemistry, Faculty of Science, Cairo University, 12613-Giza, Egypt

Corresponding author: Zafar Hussain Ibupoto,

Email: zaffar.ibhupoto@usindh.edu.pk

Abstract

The fabrication of enzyme-free glucose sensors is highly demanded for the biological, clinical and food applications. In this study, we have developed a green method for tuning the surface properties of nickel-cobalt bimetallic oxide ($NiCo_2O_4$) by adding mustard leaves extract during hydrothermal growth. The mustard leaves extract is rich with a variety of phytochemicals which can easily tune the surface properties of $NiCo_2O_4$ nanostructures, thus they have paved the way towards the development of sensitive and selective non-enzymatic glucose sensors. The effect of various amounts of mustard leaves extract (0 to 20 mL) was also studied in order to find the optimal condition for growing surface-modified $NiCo_2O_4$ nanostructures. The morphology and crystalline structure of the nanomaterials were studied by scanning electron microscopy (SEM) and powder X-ray diffraction (XRD) techniques, respectively. The presence of an increasing quantity of mustard extract keeps the crystalline structure and the morphology of the $NiCo_2O_4$ nanostructures unaltered but changes their dimensions. All nanostructures show the same cubic spinel structure of $NiCo_2O_4$ and a morphology of spherical urchins composed of nanorods, but the diameter of the urchins decreases from about 10 microns to several nanometers, increasing the surface area of the nanomaterial. Furthermore, $NiCo_2O_4$ nanostructures were deposited onto glassy carbon electrodes (CGE), showing excellent catalytic properties towards the enzyme-free detection of glucose using cyclic voltammetry. The intensity of the peak oxidation current was linear over a wide range of glucose concentrations (from 0.1 to 10 mM) and the limit of detection was estimated around 0.001 mM. $NiCo_2O_4$ nanostructures modified with 20 ml of mustard leaf extract during growth also demonstrated good repeatability and excellent selectivity of the glucose response, without any reaction to many interferers: glucose, urea, lactic acid, uric acid, ascorbic acid, potassium ions and sodium ions. The mustard leaf extract has therefore shown high potential as a green approach to improve the electrochemical properties of nanostructured materials, and could be useful for a wide range of materials for future electrochemical applications.

Keywords: Mustard leaves extract, $NiCo_2O_4$ nanostructures, enzyme-free glucose sensor, Glucose oxidation, hydrothermal method

1. Introduction

Diabetes is one of the emerging human health problems caused by unbalanced levels of glucose in the blood [1-3]. A high sugar level is a possible indicator of serious diseases like kidney failure or a precursor to heart attack and stroke; therefore it is essential to keep constant monitoring of the glucose level in human blood [1, 4-6]. Glucose monitoring is performed by means of different types of devices such as electrochemical and optical sensors [7, 8]. For real-time glucose monitoring , electrochemical sensors are preferred for their high sensitivity and fast response time. Generally, two types of glucose sensors are known: (I) glucose oxidase-based and (II) enzyme-free sensors. The first type of sensors is considered a biosensor as it involves a bioreceptor like glucose oxidase for the conversion of the biological signal into an electrical signal, whereas the second type does not use any bioreceptor, so it is considered simply a sensor. Enzyme-based glucose biosensors are highly sensitive and selective, however they are limited by the complexity of the enzyme immobilization process, high cost and long term stability issues [9-11]. On the other hand, enzyme-free sensors are free from enzyme immobilization, storage stability and high cost issues. The only challenge in the fabrication of enzyme-free glucose sensors is the requirement of an active catalytic material that can easily catalyze the glucose molecule. For this purpose, several materials have been studied for the development of enzyme-free glucose sensors, such as transition metal, alloys, noble metals and metal oxides [12-14]. Transition metal oxides exhibit excellent catalytic properties towards glucose oxidation [15-19]. The shape, size and surface morphology can greatly improve the electrochemical properties of nanostructured metal oxides [18, 20-24]. As part of the development of modern electrochemical sensors and biosensors, various materials derived from transition metals have been tested for glucose sensing applications [20, 25-28]. Single metal-based oxides have relatively poor performance in terms of low electrical conductivity, low density of catalytic sites, and poor chemical stability. Therefore, the fabrication of nanostructured materials currently focuses on bimetallic oxides and hybrid systems in order to enhance the performance of enzyme -free glucose sensors. Nickel-cobalt bimetallic oxide ($NiCO_2O_4$) exhibits excellent conductivity twice as high as that of Co_3O_4 or NiO and is studied in different fields and applications [29-31], so we focused on this material for the development of an enzyme-free glucose sensor. Various morphologies of $NiCo_2O_4$ have been studied for glucose oxidation and other related electrochemical processes, such

as nanorods [32, 33], nanowires [34], nanoneedles [35], nano/micro-spheres [36, 37], mesoporous [38], nanoflowers [39], nano wrinkles [40] and nanocages [41, 42]. Several techniques have been used to modify the surface and electrochemical properties of $NiCO_2O_4$ such as the combination with conductive carbon-based materials [43-45] and conducting polymers[46, 47].

However, there is less attention and few scientific studies on the use of biomass waste to increase the performance of $NiCO_2O_4$ via alteration of morphology, surface defects, and charge transport. Keeping in view the above facts and the uniqueness and attractive phytochemistry of mustard plant leaves, here we study for the first time the role of mustard extract in modifying the surface properties of $NiCO_2O_4$ and therefore its performance in glucose oxidation. The phytochemistry of the mustard plant includes phenolics, polyphenols, flavonoids, carotenoids and phenolic acids (zeaxthanin, lutein and β carotene), phytosterols, chlorophyll, alkaloids, glucosinolates (indoles, isothiocyanates) [48, 49].

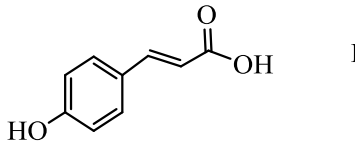

p-coumaric acid

1

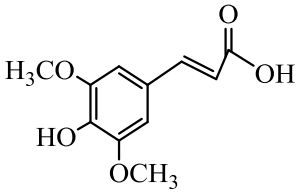

Sinapic acid

11

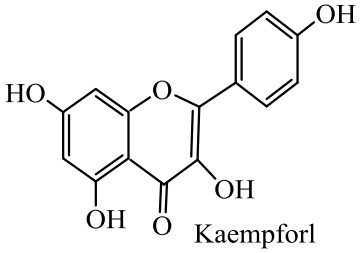

Kaempforl

111

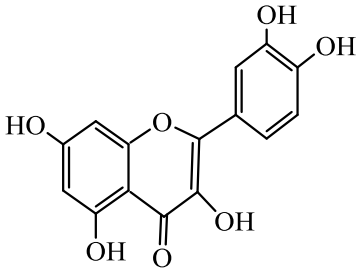

Quercetin

1V

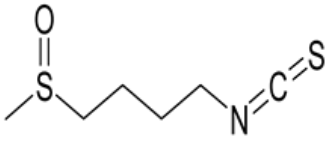

Sulforaphane

V

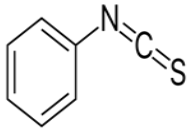

phenylisothiacynate

V1

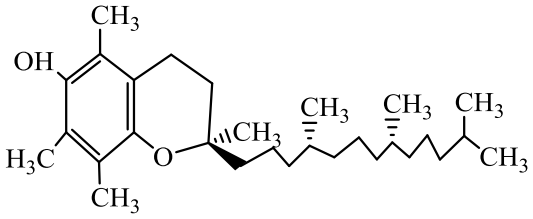

Tocopherol

V11

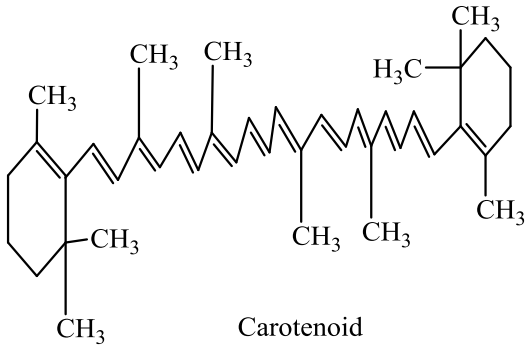

Carotenoid

V111

Scheme 1: Shows the various phytochemicals present in the mustard leaves extract

The phytochemistry of the mustard plant indicates that it is a rich source of oxidizing agents which can play a vital role in creating surface defects in $NiCO_2O_4$ nanostructures, thereby modifying the surface properties towards a more efficient surface reaction [50, 51].

In this study, we investigated the role of mustard leaves extract phytochemicals in surface modification of $NiCO_2O_4$ nanostructures. The surface modification of $NiCO_2O_4$ nanostructures was carried out with different amounts of mustard leaves extract during the hydrothermal process. The morphology of $NiCO_2O_4$ changed from bundles of nanorods to clusters of nanoparticles when the mustard leaves extract was added to the growth process. XRD and SEM were used to verify the crystalline structure and morphology of the prepared $NiCO_2O_4$ nanomaterials. Furthermore, the influence of mustard leaves extract on $NiCO_2O_4$ nanostructures was even stronger towards sensitive and selective glucose oxidation. The $NiCO_2O_4$-based glucose sensors showed a linear working range from a glucose concentration of 0.1 mM to 10 mM.

2. Materials and Methods

In the processes of nanomaterial growth and sensor testing, cobalt chloride hexahydrate ($CoCl_2 \cdot 6H_2O$), nickel chloride hexahydrate ($NiCl_2 \cdot 6H_2O$), glucose, lactic acid, uric acid, sodium chloride, potassium chloride, ascorbic acid, sodium hydroxide and urea were used. All chemicals were of standard quality and were used as purchased from Sigma Aldrich Karachi, Pakistan, without further purification. For the standard growth of bimetallic oxide nanostructures, 0.1 M cobalt chloride hexahydrate and 0.1 M nickel chloride hexahydrate were added to 100 mL of deionized water using 0.1 M urea as the hydroxide source. The solution was then divided into five beakers in order to have different growth processes. Fresh green mustard leaves were cleaned with deionized water, dried and chopped. The pieces of leaves were placed in a domestic juicer machine and the juice was extracted. Nothing was added to the first beaker, so that it served as a reference for the growth of pure bimetallic cobalt-nickel oxide. In the other four beakers, 5, 10, 15 and 20 mL of mustard leaf extract were added respectively, and the final nanomaterials were named Sample 1, 2, 3 and 4, respectively. All the solutions in the five beakers were mechanically stirred, homogenized and then hermetically sealed with aluminum foil and left in an electric oven preheated to 90 - 95 ° C for 5 - 6 h for the hydrothermal growth process. At the end of the growth process, the nickel-cobalt hydroxide was collected on filter paper and allowed to dry overnight. Then a thermal annealing of 5 hours at 500 °C in air was carried out in order to obtain $NiCo_2O_4$ material.

The morphology of the $NiCo_2O_4$ nanomaterials was studied by scanning electron microscopy (SEM) at an accelerating voltage of 10 kV, while its crystalline structure was studied by means of powder X-ray diffraction with CuKα radiation (λ = 1.5418 Å) using a potential of 45 kV and a current of 45 mA. Cyclic voltammetry and amperometry were used to test the performance of electrochemical sensors. The measurement setup was as follows: 10 mg of $NiCo_2O_4$ nanomaterial were dissolved in 2.5 mL of deionized water and 0.5 mL of Nafion (5%) and sonicated until a uniform suspension was obtained. The glassy carbon electrode (GCE, 3 mm) was polished with aluminum paste and then washed with deionized water. The modification of the GCE electrodes with the various $NiCo_2O_4$ nanomaterials was carried out using the drop casting method. Bare GCE and those modified with nanomaterials were used as working electrodes for glucose detection. In the three-electrode arrangement, platinum wire was used as counter electrode, GCE as working electrode and silver- silver chloride (Ag/AgCl) saturated with KCl (3M) was used as reference

electrode. A stock solution of 50 mM glucose was prepared in 0.1M NaOH. All glucose measurements were performed in NaOH used as an alkaline electrolyte. The dilution method was used to prepare lower concentration solutions starting from the glucose stock solution. For selectivity studies, a 0.1 mM solution of each interfering substance (glucose, urea, lactic acid, uric acid, ascorbic acid, potassium ions, sodium ions) was prepared in deionized water and its effect on the enzyme-free sensor was monitored under alkaline NaOH conditions. The limit of detection was estimated via published method [52].

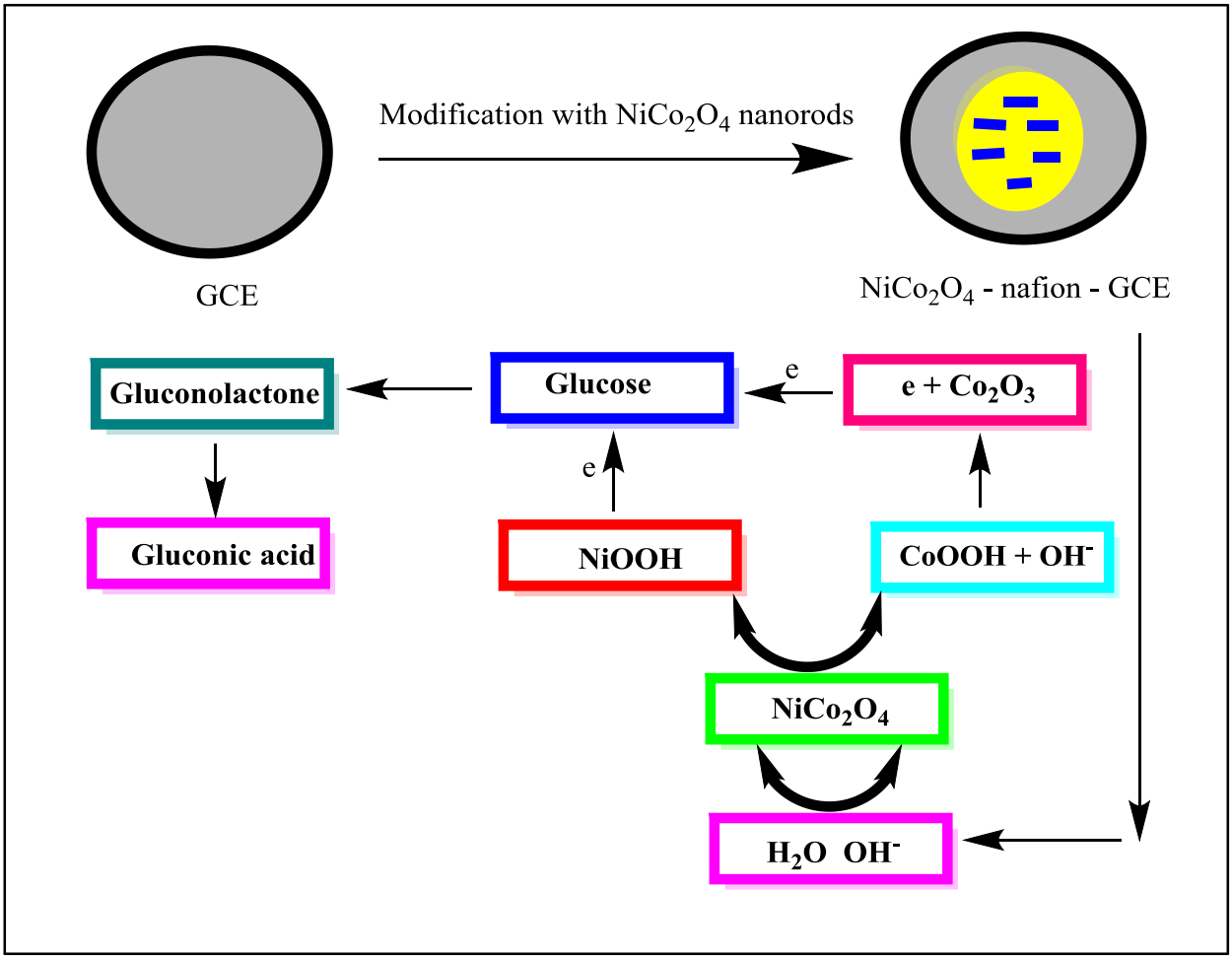

Scheme 2: Modification of GCE and sensing mechanism of glucose under alkaline NaOH conditions by $NiCo_2O_4$ nanomaterials prepared with mustard leaves extract

3. Results and Discussion

3.1. Structure and morphology of $NiCO_2O_4$ nanostructures

The crystalline structure of $NiCO_2O_4$ nanostructures prepared with different quantities of mustard leaves extract (5, 10, 15 and 20 mL) was investigated by means of powder XRD, and the patterns are shown in Figure 1. In the lower part of the figure, as a reference, there is also the pattern of pure $NiCO_2O_4$ grown without mustard extract. The main diffraction peaks are visible at 19.4°, 31.3°, 36.88°, 38.59°, 44.85°, 59.41° and 65.30°, which could be respectively indexed to the crystalline planes (111), (220), (311), (222), (400), (511) and (440) of the spinel $NiCO_2O_4$ reported in the JCPDS 01-073-1702 reference sheet and shown at the bottom of Fig. 1. Comparing the patterns of the different samples we can see how, although the peaks relative to $NiCO_2O_4$ are always visible, when the quantity of mustard extract added to the growth increases, the intensity of the peaks decreases. Furthermore, the relative intensities between the peaks change, and a slight shift in the position of the peaks is also observed. The modification of these parameters demonstrates the effect of mustard extract on the hydrothermal growth of $NiCO_2O_4$ nanostructures, which it could be attributed to the presence of a broad spectrum of macromolecules and phytochemicals from mustard leaves. SEM analysis was used to evaluate the shape and size of the various $NiCO_2O_4$ nanostructures grown with different amounts of mustard extract and the SEM images of the samples are shown in Figure 2. Pristine $NiCO_2O_4$ nanostructures (grown without mustard extract) appear as urchins composed of nanorods, as shown in Figure 2a. The length of the pristine $NiCO_2O_4$ nanorods was about 10 μm, while their average diameter was about half a micron. Comparing the SEM images of the nanostructures grown with increasing quantities of mustard extract (Samples 1-4 in Fig. 2c-f it is noted that the shape and size change. As the quantity of mustard extract in the hydrothermal process increases from 0 to 20 mL, the nanostructures produced become smaller: urchins are smaller because they are composed of thinner and shorter nanorods. The diameter of the urchins in fact decreases from about 10 μm in Fig. 2a (pristine $NiCO_2O_4$) to about few nm in Fig. 2f ($NiCO_2O_4$ with 20 mL of mustard extract). The nanorods that make up urchins also become shorter and thinner, passing from 10 μm to some nm. This change in size, which leads to a greater surface area and therefore improves sensor performance, is attributable to the presence of phytochemicals from the mustard leaf extract during the growth, which played a crucial role in reducing the size of the $NiCO_2O_4$ nanostructures from microns to nanometers.

The process of formation of $NiCO_2O_4$ nanostructures in the hydrothermal method occurs through the hydrolysis of urea and the formation of metal-hydroxyl bonds. The step-by-step synthesis mechanism of $NiCO_2O_4$ is illustrated in the following reactions:

$$NH_2CONH_2 + H_2O \rightarrow 2\ NH_3 + CO_2 \quad (1)$$

$$NH_3 + H_2O \rightarrow NH_4^+ + OH^- \quad (2)$$

$$Ni^{2+} + CO^{2+} + 6OH^- \rightarrow [\ NiCO(OH)_6\ ] \quad (3)$$

$$[\ NiCO(OH)_6\ ] \rightarrow NiCO_2O_4 + H_2O + H_2 \quad (4)$$

In the first reaction the hydrolysis of urea leads to the formation of ammonia, which in the second reaction leads to the production of hydroxyl ions through the reaction of water with ammonia. Then, cobalt and nickel metal ions react with hydroxyl ions giving rise to the formation of the bimetallic hydroxide described in reaction (3). In the last reaction the bimetallic hydroxide is finally transformed into bimetallic oxide $NiCO_2O_4$, which is the final produc [53, 54].

3.2. Glucose oxidation on $NiCO_2O_4$ nanostructures prepared with mustard leaves extract

Cyclic voltammetry was used to evaluate the electrochemical behavior in alkaline conditions of the different $NiCO_2O_4$ nanostructures grown with different quantities of mustard leaves extract. Voltammograms for the four samples and the reference grown without mustard extract are shown in Figure 3a. Figure 3b shows the voltammogram of bare GCE and GCE modified with Sample 4 ($NiCO_2O_4$ nanostructures grown with 20 mL of mustard extract) in aqueous solution of 0.1 M NaOH, in the absence and presence of 0.1 mM of glucose.

It is clear that in the case of bare GCE there is no response, i.e. the material is inactive as regards the oxidation of glucose. On the other hand, when GCE is modified with $NiCO_2O_4$ nanostructures grown with the addition of mustard leaf extract, the response to the presence of glucose is remarkable. To better understand the effects of mustard leaf extract during growth on the detection

properties of bimetallic oxide, we tested the four samples grown with different amounts (0 to 20 mL) in the presence of glucose. Figure 3a shows the CV curves obtained with pure $NiCO_2O_4$ and the samples grown with 5, 10, 15 and 20 mL of mustard leaf extract in a 0.1 mM glucose solution. It is clear that the presence of a greater quantity of mustard extract during hydrothermal growth makes the $NiCO_2O_4$ nanostructures more sensitive to glucose oxidation. Based on the voltammograms shown in Figure 3a, we decided to further study the parameters of the enzyme-free glucose sensor based on $NiCO_2O_4$ nanostructures prepared with 20 ml of mustard leaf extract.

The detection mechanism of the enzyme-free glucose sensor based on $NiCO_2O_4$ can be described by a series of redox reactions whereby the electrons produced by the oxidation of glucose are collected by the nanostructures of $NiCO_2O_4$ producing an electrical signal. In the alkaline electrolyte, the $NiCO_2O_4$ nanostructures are transformed into nickel and cobalt hydroxides and at the same time the glucose is oxidized to gluconolactone as shown in the following chemical reactions [16, 17].

$$NiCo_2O_4 + OH^- + H_2O \rightarrow \quad NiOOH + 2COOH + e \qquad (5)$$

$$CoOOH + OH^- \rightarrow Co_2O_3 + H_2O + e \qquad (6)$$

$$NiOOH + Glucose \rightarrow Ni(OH)_2 + Gluconolactone \qquad (7)$$

$$CoOOH + Glucose \rightarrow Co(OH)_2 + Gluconolactone \qquad (8)$$

$$Ni^{2+} + Co^{2+} \rightarrow \ Ni^{3+}\ Co^{3+} + 2e \qquad (9)$$

$$Glucose\ (C_6\ H_{12}\ O_6) \rightarrow Gluconolactone\ (C_6\ H_{10}\ O_6) + 2H^+ + 2e \qquad (10)$$

The detection mechanism of the $NiCo_2O_4$ glucose sensor is based on the reduction of Ni^{3+} and Co^{3+} to Ni^{2+} and Co^{2+} by gaining electrons during glucose oxidation. The smaller dimensions of the nanorods in the samples grown with a greater quantity of mustard extract give the electrode a greater surface area, also aided by the hierarchical structure of the urchins composed of thinner

nanorods, allowing a rapid transfer of electrons between the glucose molecules and the electrode. To confirm the electron transfer kinetics, voltammograms were performed in 0.1 mM glucose solution at increasing scan rates, as shown in Figure 4a. The anode peak current and cathode peak current increase as the scan rate increases, suggesting that $NiCo_2O_4$ has reversible reaction characteristics and that reactions on the $NiCo_2O_4$-modified GCE are diffusion controlled. This is confirmed by the linearity of the anode peak current versus scan rate graph shown in Figure 4b.

To study the linearity of the sensor response, CV curves were made at various glucose concentrations, from 0.1 to 10 mM, as shown in Figure 5a. The peak anode current was plotted against the glucose concentration in Fig. 5b, showing that the sensor responds linearly over the entire 0.1 - 10 mM concentration range. The linear graph of peak current versus glucose concentration confirms that the enzyme-free sensor has excellent analytical ability to measure glucose with high precision and accuracy, as confirmed by the regression coefficient value of 0.99 shown in Figure 5b. The detection limit of the glucose sensor was found to be 0.001 mM. The linear glucose detection range confirms the sensor's ability to accurately monitor glucose concentrations typical of physiological conditions 5-6 mM.

In the development of sensors for specific applications, selectivity is one of the main parameters for evaluating the performance of a sensor towards the target analyte with respect to possible interferers. For this purpose we investigated the sensor response to urea, lactic acid, uric acid, ascorbic acid, K+ ions and Na+ ions compared to that to glucose. To compare the responses also in a quantitative way, all substances were measured at the same glucose concentration (0.1 mM), and the curves are shown in Figure 6a. Only glucose produced a response, while the other substances produced no effect on the oxidation signal, therefore $NiCo_2O_4$-modified GCE grown with 20 mL of mustard extract demonstrated a highly selective response towards glucose.

Another important property for a sensor is repeatability, which reflects the chemical and mechanical stability of the materials. Theoretically, one of the positive aspects of an enzyme-free sensor is its intrinsic stability due to the lack of involvement of bioreceptors (which are much more delicate) since the signal derives from the catalytic nature of the materials used.

However, the $NiCo_2O_4$ nanostructures could detach from the GCE, and it is therefore useful in any case to study the repeatability of the sensor. For this reason the sensor was tested with 20measurement cycles with a glucose concentration of 0.1 mM, and the results are shown in Figure 6b. The plots obtained in the various cycles are practically superimposed in the

Figuredemonstrating that there is no substantial change in the peak glucose oxidation current and no shift in the peak potential. This means that the $NiCo_2O_4$ nanostructures grown with the mustard leaf extract are firmly bound to the GCE, giving stability to the sensor. Furthermore, the stability of the sensor was also studied by chronoamperometry for a few hours, as shown in Figure 6c. The results of the experiment revealed high stability, confirming the conclusions drawn from the CV results.

The results regarding the response, limit of detection, linear range of response, selectivity and stability of the manufactured glucose sensor confirm that $NiCo_2O_4$ nanostructures prepared with mustard leaf extract have a high potential as sensing material for glucose in biomedical applications. The performances obtained are equal or superior to those recently reported in scientific literature by enzyme-free glucose sensors, shown in Table 1. Furthermore, the approach to the growth of $NiCo_2O_4$ nanostructures presented here is simple, elogical and low cost.

Table 1: Performance comparison of the enzyme-free sensor based on $NiCo_2O_4$ nanostructures grown with 20 mL mustard leaf extract versus several non-enzymatic glucose sensors in the literature.

Sensing electrode	Sensitivity ($\mu AmM^{-1}cm^{-2}$)	Linear Range (mM)	LOD (μM)	Reference
RGO-$Ni(OH)_2$ nanoplates	11.43	0.002 - 3.1	0.6	[55]
Co_3O_4 hollow nanododecahedra	708.4	0.002 - 6.02	0.58	[56]
GO- templated NiO nanosheets	1138	0.001 - 0.4	0.18	
$NiCo_2O_4$ nanorods	4710	0.001 – 0.88	0.063	[32]
$NiCo_2O_4$ nanospheres	1917	0.01 – 0.3	0.6	[36]
Ni-SnO_x/PANI/CuO	1625 & 1325	0.001-1 & 1-10	0.130	[57]
Au@Cu_2O	715	0.05-2.0	18	[58]
Pt-Pd nanoparticles	24	2-12	1.0	[59]
rGO-PtNW	56.11	0.032-1.89	4.6	[60]
Au/rGO/AuPt/GO_x/Nafion	82	0.1-2.3	N/A	[61]
CuO-6/GCE	992.073 & 541.75	0.001-1.164 & 1.164-5.664	0.307	[62]
NiFe-LDH/NF	3680.2	0.002-0.8	0.59	[63]
MXene/NiCo-LDH/GCE	64.75	0.002-4.096	0.53	[64]
$NiCo_2O_4$ with mustard leave extract	-	-0.1 - 10	1	This work

4. Conclusions

In this study we used a green approach to grow hierarchical $NiCo_2O_4$ nanostructures using mustard leaf extract during the hydrothermal process, to be used as a glucose sensor. Various quantities of

mustard leaf extract were used (0 to 20 mL) to understand its effects on the size and morphology of the $NiCo_2O_4$ nanostructures. The results show that the phytochemicals in the mustard leaf extract successfully changed the size of the $NiCo_2O_4$ nanostructures from several micrometers to nanometers, greatly increasing the sensor surface area. The optimized $NiCo_2O_4$ nanostructures with 20 ml of mustard leaf extract showed a strong oxidation peak during glucose detection. The enzyme-free sensor exhibited a linear working range for glucose concentrations from 0.1 to 10 mM and a detection limit of approximately 0.001 mM. Furthermore, the device demonstrated very good selectivity to glucose with respect to several interferers (glucose, urea, lactic acid, uric acid, ascorbic acid, potassium ions, sodium ions) and good stability. The results of the present study strongly motivate the use of mustard leaf extract to fine-tune the surface properties of a wide range of materials to be used for specific electrochemical applications.

Acknowedgement

We extend sincere appreciation to the Researchers Supporting Project (RSP-2022/79) at King Saud University, Riyadh, Saudi Arabia.

Author's contribution

Abdul Ghaffar Solangi, did material synthesis and carried out preliminary testing

Tajness Pirzada, did partial supervision of work

Aqeel Ahmed Shah, did XRD measurement

Abdul Sattar Chang, did partial electrochemical sensing,

Zulifqar Ali Solangi, did SEM analysis

Muhammad Yameen Solangi, did partial electrochemical measurement

Umair Aftab, provided the access to electrochemical testing

Matteo Tonezzer, did editing and preview the draft of manuscript

Aneela Tahira, did XRD analysis

Shymaa S. Medany, participated in the results discussion

Ayman Nafady, did the proofreading of work

Zafar Hussain Ibupoto, designed the research study and supervised the work, and edited the first draft of manuscript

Conflict of Interest statement

Authors declare no conflict of interest in this research work

5. References

1. A. Abellán-Llobregat, I. Jeerapan, A. Bandodkar, L. Vidal, A. Canals, J. Wang and E. Morallon, *Biosensors and Bioelectronics*, 2017, **91**, 885-891.
2. N. Cho, J. Shaw, S. Karuranga, Y. Huang, J. da Rocha Fernandes, A. Ohlrogge and B. Malanda, *Diabetes research and clinical practice*, 2018, **138**, 271-281.
3. S. O. Song, Y. D. Song, J. Y. Nam, K. H. Park, J.-H. Yoon, K.-M. Son, Y. Ko and D.-H. Lim, *Diabetes & metabolism journal*, 2016, **40**, 35-45.
4. A. A. Ensafi, N. Zandi-Atashbar, B. Rezaei, M. Ghiaci and M. Taghizadeh, *Electrochimica Acta*, 2016, **214**, 208-216.
5. A. J. Bandodkar and J. Wang, *Trends in biotechnology*, 2014, **32**, 363-371.
6. H. Yao, Y. Liao, A. Lingley, A. Afanasiev, I. Lähdesmäki, B. Otis and B. Parviz, *Journal of Micromechanics and Microengineering*, 2012, **22**, 075007.
7. J. S. Chung and S. H. Hur, *Sensors and Actuators B: Chemical*, 2016, **223**, 76-82.
8. D.-M. Kim, J.-M. Moon, W.-C. Lee, J.-H. Yoon, C. S. Choi and Y.-B. Shim, *Biosensors and Bioelectronics*, 2017, **91**, 276-283.
9. X. Bo, J. C. Ndamanisha, J. Bai and L. Guo, *Talanta*, 2010, **82**, 85-91.
10. W.-Z. Jia, K. Wang, Z.-J. Zhu, H.-T. Song and X.-H. Xia, *Langmuir*, 2007, **23**, 11896-11900.
11. J. Wang, *Electroanalysis: An International Journal Devoted to Fundamental and Practical Aspects of Electroanalysis*, 2001, **13**, 983-988.
12. A. Martins, V. Ferreira, A. Queirós, I. Aroso, F. Silva and J. Feliu, *Electrochemistry communications*, 2003, **5**, 741-746.
13. X. Niu, M. Lan, C. Chen and H. Zhao, *Talanta*, 2012, **99**, 1062-1067.
14. J. Yuan, K. Wang and X. Xia, *Advanced Functional Materials*, 2005, **15**, 803-809.
15. G. Li, H. Huo and C. Xu, *Journal of Materials Chemistry A*, 2015, **3**, 4922-4930.
16. K. K. Naik, S. Kumar and C. S. Rout, *RSC Advances*, 2015, **5**, 74585-74591.
17. K.-b. Jang, K. R. Park, K. M. Kim, S.-k. Hyun, J.-e. Jeon, Y. S. Song, S.-k. Park, K.-i. Moon, C. Ahn and S.-c. Lim, *Nanomaterials*, 2021, **11**, 55.
18. C. Yuan, H. B. Wu, Y. Xie and X. W. Lou, *Angewandte Chemie International Edition*, 2014, **53**, 1488-1504.
19. Z. Wu, Y. Zhu and X. Ji, *Journal of Materials Chemistry A*, 2014, **2**, 14759-14772.
20. S. Amin, A. Tahira, A. Solangi, V. Beni, J. Morante, X. Liu, M. Falhman, R. Mazzaro, Z. H. Ibupoto and A. Vomiero, *RSC advances*, 2019, **9**, 14443-14451.
21. S. Chen, W. Xing, J. Duan, X. Hu and S. Z. Qiao, *Journal of materials chemistry a*, 2013, **1**, 2941-2954.
22. S. K. Meher and G. R. Rao, *The Journal of Physical Chemistry C*, 2011, **115**, 15646-15654.
23. G. R. Patzke, Y. Zhou, R. Kontic and F. Conrad, *Angewandte Chemie International Edition*, 2011, **50**, 826-859.
24. C. Rao, *Journal of Materials Chemistry*, 1999, **9**, 1-14.
25. K. Dick, 2008.
26. U. Yogeswaran and S.-M. Chen, *Sensors*, 2008, **8**, 290-313.

27. M. Vidotti, S. I. C. de Torresi and L. T. Kubota, *Sensors and Actuators B: Chemical*, 2008, **135**, 245-249.
28. M. Arain, A. Nafady and Z. Sirajuddin, *Shaikh, H. Khan, A. Alsalme, A. Niaz and M. Willander, RSC Adv*, 2016, **6**, 39001-39006.
29. R. Ding, L. Qi, M. Jia and H. Wang, *Nanoscale*, 2014, **6**, 1369-1376.
30. M. A. Prathap, B. Satpati and R. Srivastava, *Electrochimica Acta*, 2014, **130**, 368-380.
31. L. Qian, L. Gu, L. Yang, H. Yuan and D. Xiao, *Nanoscale*, 2013, **5**, 7388-7396.
32. M. Saraf, K. Natarajan and S. M. Mobin, *New Journal of Chemistry*, 2017, **41**, 9299-9313.
33. J. Yang, M. Cho and Y. Lee, *Biosensors and Bioelectronics*, 2016, **75**, 15-22.
34. Q. Guo, W. Zeng and Y. Li, *Materials Letters*, 2019, **256**, 126603.
35. L. Liu, Z. Wang, J. Yang, G. Liu, J. Li, L. Guo, S. Chen and Q. Guo, *Sensors and Actuators B: Chemical*, 2018, **258**, 920-928.
36. W. Huang, Y. Cao, Y. Chen, J. Peng, X. Lai and J. Tu, *Applied Surface Science*, 2017, **396**, 804-811.
37. H. Yin, T. Zhan, D. Qin, X. He, Q. Nie and J. Gong, *Inorganic and Nano-Metal Chemistry*, 2017, **47**, 1560-1567.
38. P. Arunachalam, M. A. Ghanem, A. M. Al-Mayouf and M. Al-shalwi, *Materials Letters*, 2017, **196**, 365-368.
39. Z. Lu, L. Wu, J. Zhang, W. Dai, G. Mo and J. Ye, *Materials Science and Engineering: C*, 2019, **102**, 708-717.
40. G. Ma, M. Yang, C. Li, H. Tan, L. Deng, S. Xie, F. Xu, L. Wang and Y. Song, *Electrochimica Acta*, 2016, **220**, 545-553.
41. Y. Feng, D. Xiang, Y. Qiu, L. Li, Y. Li, K. Wu and L. Zhu, *Electroanalysis*, 2020, **32**, 571-580.
42. Y. Li, B. Liu, H. Wang, X. Su, L. Gao, F. Zhou and G. Duan, *Science China Materials*, 2018, **61**, 1575-1586.
43. S. Xu, D. Yang, F. Zhang, J. Liu, A. Guo and F. Hou, *Rsc Advances*, 2015, **5**, 74032-74039.
44. A. Espinosa, J. Kolosnjaj-Tabi, A. Abou-Hassan, A. Plan Sangnier, A. Curcio, A. K. Silva, R. Di Corato, S. Neveu, T. Pellegrino and L. M. Liz-Marzán, *Advanced Functional Materials*, 2018, **28**, 1803660.
45. L. Chang, C. Li, H. Ouyang, J. Huang, Q. Huang and Z. Xu, *Materials Letters*, 2019, **240**, 21-24.
46. J. Chen, T. Ma, M. Chen, Z. Peng, Z. Feng, C. Pan, H. Zou, W. Yang and S. Chen, *Journal of Energy Storage*, 2020, **32**, 101895.
47. M. Peng, X. Tian, D. Li, Q. Wang and D. Zhang, *Materials Letters*, 2020, **272**, 127859.
48. S. Argento, M. G. Melilli and F. Branca, *Agronomy*, 2019, **9**, 820.
49. K. M. Favela-González, A. Y. Hernández-Almanza and N. M. De la Fuente-Salcido, *Journal of Food Biochemistry*, 2020, **44**, e13414.
50. H. Nawaz, M. A. Shad and A. Rauf, *Food chemistry*, 2018, **242**, 182-187.
51. S. M. Mandal, D. Chakraborty and S. Dey, *Plant signaling & behavior*, 2010, **5**, 359-368.
52. S. Amin, A. Tahira, A. R. Solangi, R. Mazzaro, Z. H. Ibupoto, A. Fatima and A. Vomiero, *Electroanalysis*, 2020, **32**, 1052-1059.
53. Z.-Q. Liu, K. Xiao, Q.-Z. Xu, N. Li, Y.-Z. Su, H.-J. Wang and S. Chen, *Rsc Advances*, 2013, **3**, 4372-4380.
54. P. Nayak, M. Sahoo and S. K. Nayak, *Ceramics International*, 2020, **46**, 3818-3826.
55. Y. Zhang, F. Xu, Y. Sun, Y. Shi, Z. Wen and Z. Li, *Journal of Materials Chemistry*, 2011, **21**, 16949-16954.
56. E. Zhang, Y. Xie, S. Ci, J. Jia and Z. Wen, *Biosensors and Bioelectronics*, 2016, **81**, 46-53.
57. A. Sedighi, M. Montazer and S. Mazinani, *Biosensors and Bioelectronics*, 2019, **135**, 192-199.
58. Y. Su, H. Guo, Z. Wang, Y. Long, W. Li and Y. Tu, *Sensors and Actuators B: Chemical*, 2018, **255**, 2510-2519.

59. M. Hossain and J. Y. Park, *Electroanalysis*, 2014, **26**, 940-951.
60. N. Muthuchamy, A. Gopalan and K.-P. Lee, *RSC advances*, 2018, **8**, 2138-2147.
61. S. Pakapongpan and R. P. Poo-Arporn, *Materials Science and Engineering: C*, 2017, **76**, 398-405.
62. P. Yang, X. Wang, C.-y. Ge, X. Fu, X. Y. Liu, H. Chai, X. Guo, H.-C. Yao, Y. X. Zhang and K. Chen, *Applied Surface Science*, 2019, **494**, 484-491.
63. Y. Lu, B. Jiang, L. Fang, S. Fan, F. Wu, B. Hu and F. Meng, *Electroanalysis*, 2017, **29**, 1755-1761.
64. M. Li, L. Fang, H. Zhou, F. Wu, Y. Lu, H. Luo, Y. Zhang and B. Hu, *Applied Surface Science*, 2019, **495**, 143554.

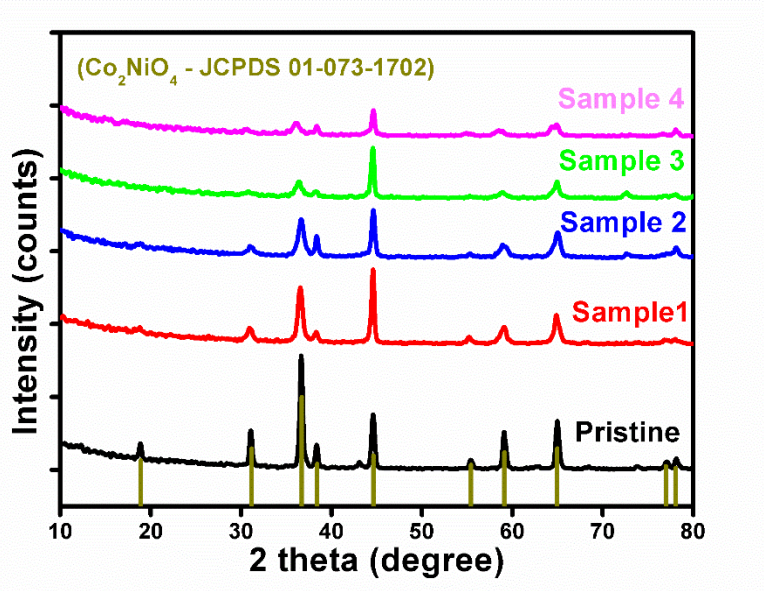

Fig. 1. XRD patterns of $NiCo_2O_4$ nanomaterials grown with different amounts of mustard leaves extract (from 0 to 20 mL).

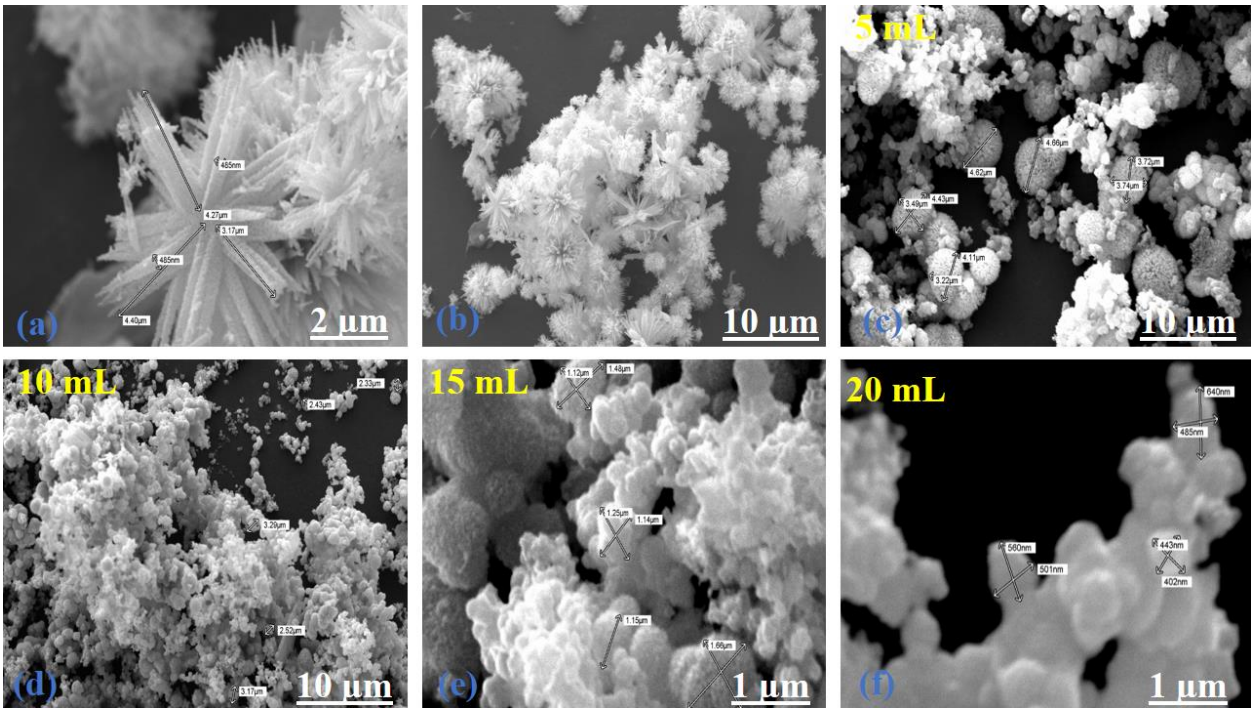

Fig. 2: SEM images of **(a, b)** pristine $NiCo_2O_4$ nanomaterial (grown with no mustard extract), **(c-f)** SEM image of $NiCo_2O_4$ nanomaterials prepared with 5, 10, 15 and 20 mL of mustard leaves extract.

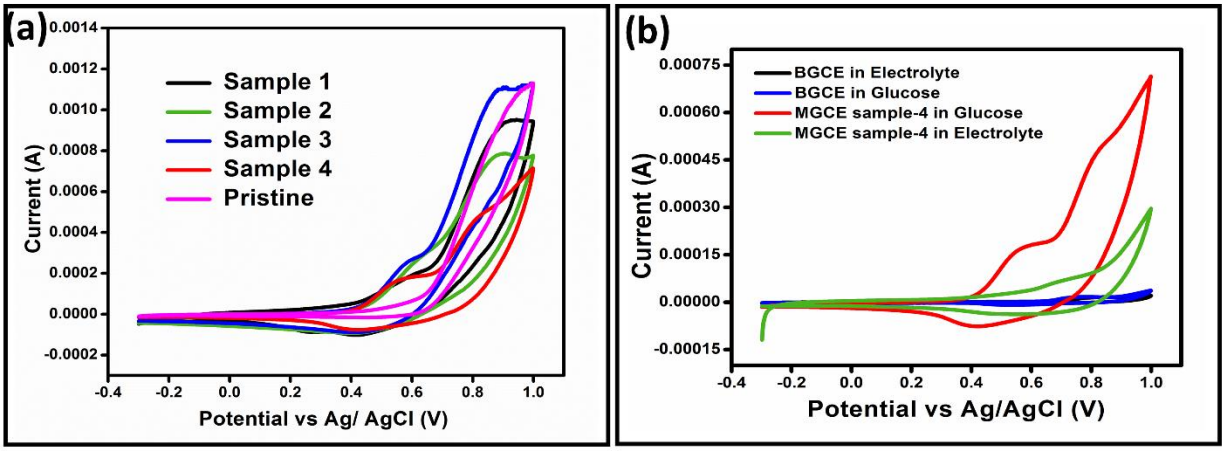

Fig. 3. (a) Cyclic voltammograms of MGCE of Sample 1, Sample 2, Sample 3, Sample 4 and pristine $NiCO_2O_4$-modified GCE in the presence of 0.1 mM of glucose at a scan rate of 50 mV/s, **(b)** Cyclic voltammogram of bare GCE in electrolyte and in the presence of glucose, and of GCE modified with Sample 4 in the presence of glucose at a scan rate of 50 mV/s.

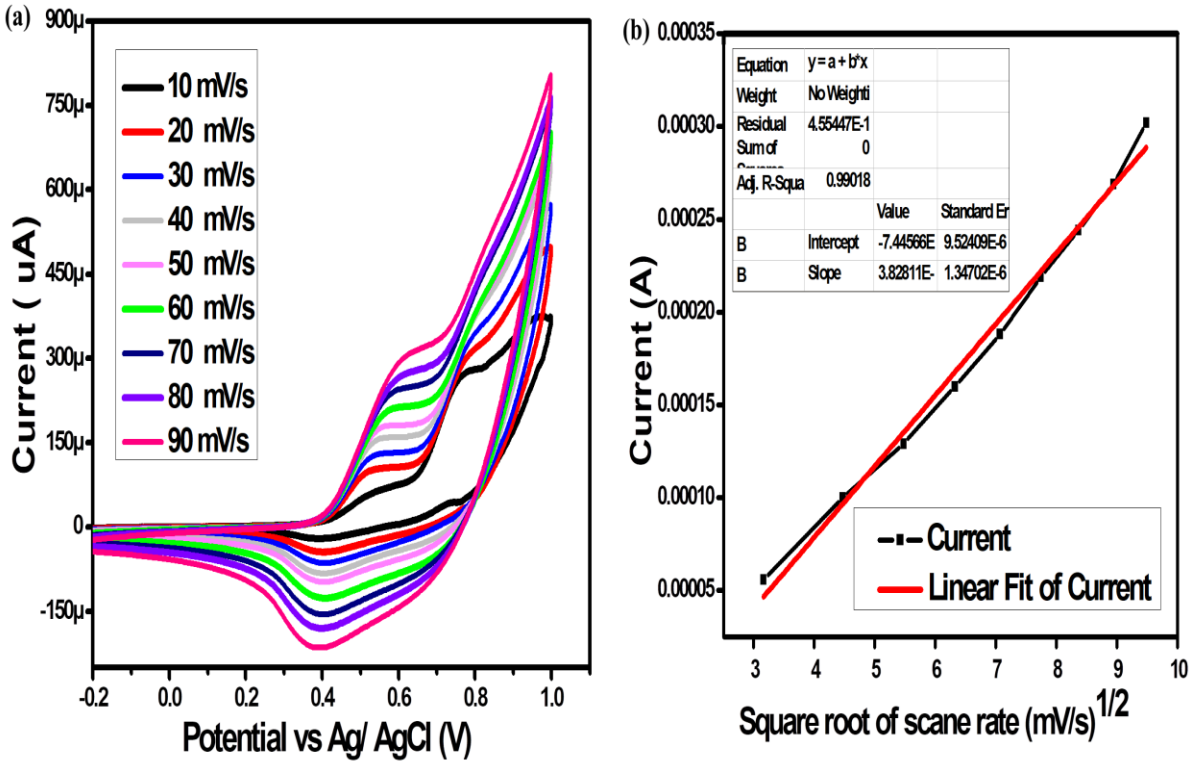

Fig. 4. (a) Cyclic voltammograms of Sample 4 collected in 0.1 mM glucose solution at different scan rates; **(b)** sensor anodic current as a function of the square root of scan rate.

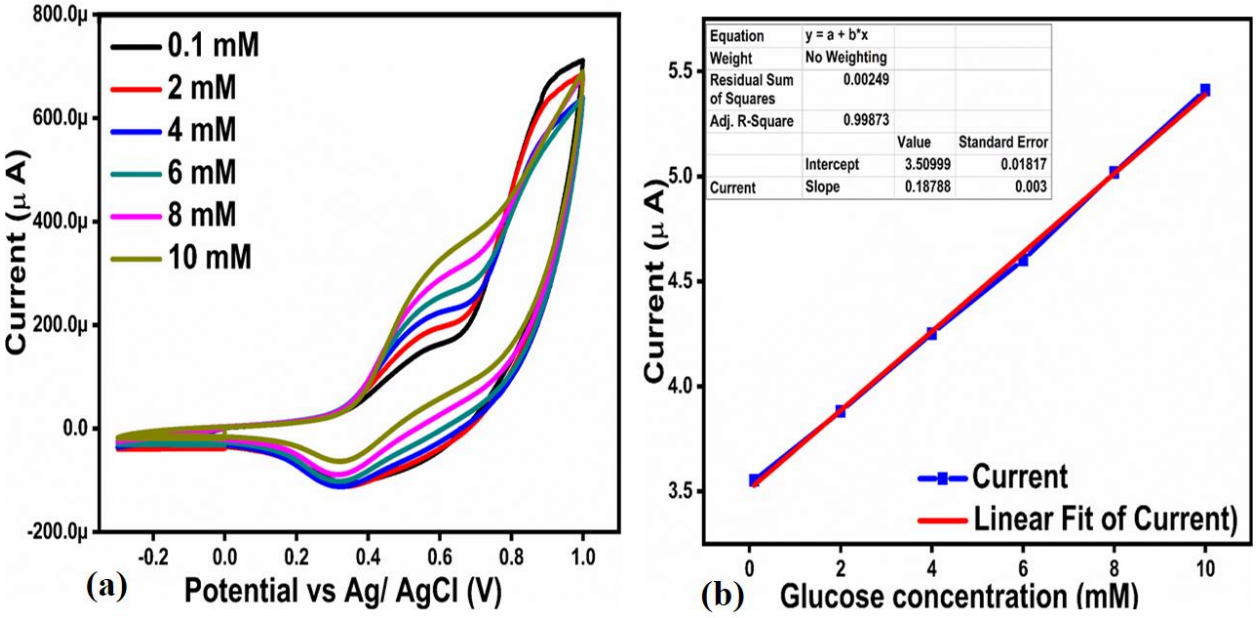

Fig. 5 (a) Cyclic voltammograms for sample 4 at different glucose concentrations at a scan rate of 50 mV/s, ; **(b)** sensor anodic current as a function of glucose concentration.

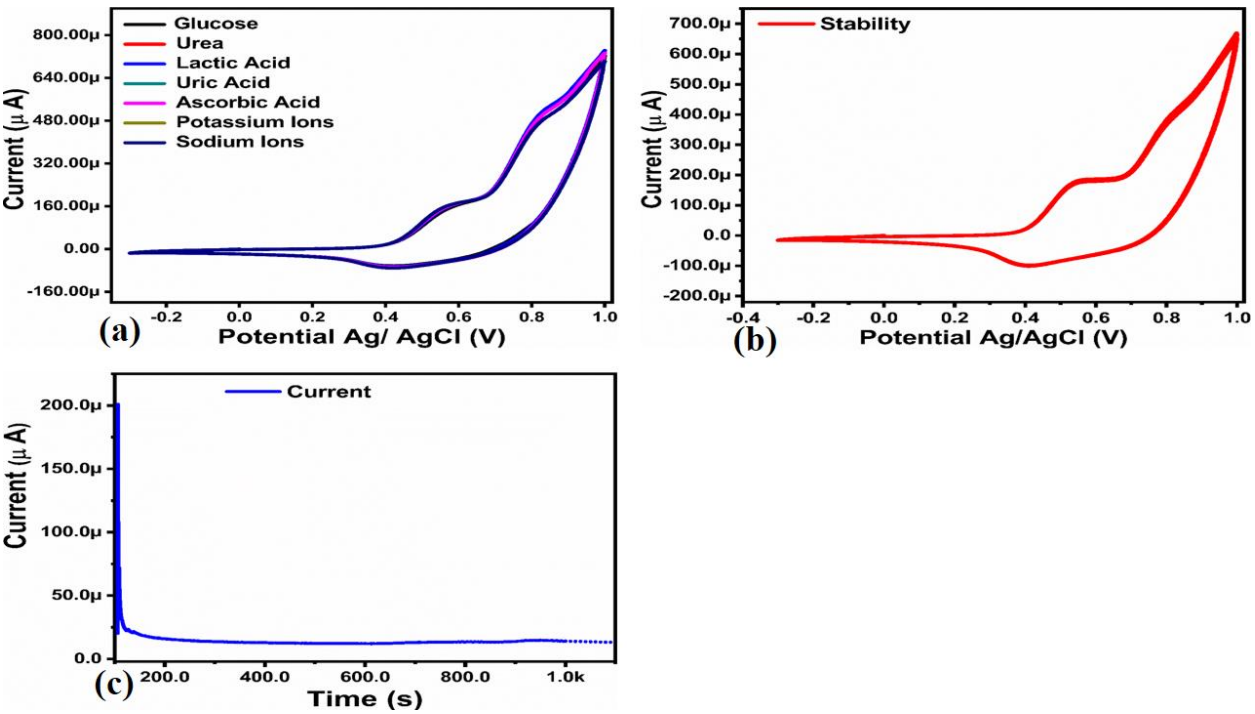

Fig. 6. (a) Cyclic voltammograms of Sample 4 collected in presence of 0.1 mM solutions of several potential interferers at a scan rate of 50 mV/s, ; **(b)** Stability study of Sample 4 collecting 20 cycles in presence of 0.1 mM of glucose at a scan rate of 50 mV/s, **(c)** i-t curve collected in presence of 0.1 mM glucose solution of at 0.56 V potential against Ag/AgCl shows the durability for the sample 4.